POLITECNICO
MILANO 1863

SCUOLA DI INGEGNERIA INDUSTRIALE
E DELL'INFORMAZIONE

Executive Summary of the Thesis

States and parameters estimation in the post-capture scenario of a spacecraft with flexible manipulator

Laurea Magistrale in Space Engineering - Ingegneria Spaziale

Author: Davide Degavi

Advisor: Prof. Mauro Massari

Co-advisors: Prof. Pierluigi Di Lizia, Prof. Riccardo Vescovini

Academic year: 2021-2022

1. Introduction

The ever-increasing number of space debris may put at risk the accessibility of space in the future. The recent development of large constellations means that, even with the proper mitigation strategies, the number of unwanted objects orbiting Earth will rapidly increase. To revert the trend, missions such as Active Debris Removal (ADR) and On-Orbit Servicing (OOS) are required. They strive to reduce space debris by adopting different strategies: ADR plans to move large, mostly intact, satellites to orbits with a fast natural decay, and OOS aims to increase the operational life of existing satellites.
Within the aforementioned framework, the ESA's e.Deorbit mission was conceptualized. The e.Deorbit mission aims to develop a multipurpose vehicle capable of performing both OOS and ADR missions, since the two mission types have numerous requirements and tasks in common.
One critical phase that OOS and ADR have in common is the post-capture phase. This scenario has seen less analyses than other phases, especially when the flexibility effects are considered. In most researches, like the one proposed by Raina et al. [4], the manipulator is the only component modelled including flexibility effects. Neglecting the effects of large flexible appendices could decrement the performance of attitude and parameter estimation algorithms. The work presented by Meng et al. [3] is one of the most comprehensive studies on the effects of flexibility for the control stability in the post-capture phase.
This work aims to further increase the knowledge of the effects of flexible space structures in the post-capture phase of an ADR or OOS mission. The main focus is on the attitude and mass parameter estimation process through the use of Kalman filtering techniques. In particular, the Extended Kalman Filter (EKF) and the Multiplicative Extended Kalman Filter (MEKF) will be considered.
Another contribution of this study is the extensive usage of the Functional Mock-up Interface (FMI) [1] for the estimation process.

2. Model implementation

The model includes a chaser linked to the ESA's derelict satellite (Envisat), through a seven degrees-of-freedom (DoFs) manipulator. Both satellites have flexible solar panels. In order to model the flexibility effects, the solar panel is

discretized in a finite number of rigid sections connected through joints with a spring-damper element. The 7 DoF manipulator has only joint flexibility.
The first methodology considered to implement the system's model was the Euler-Lagrange formalism. Although such an approach would give the smallest number of equations to describe the system dynamics, the use of this method was found to be inefficient. The reason stands with the necessity to use symbolic manipulation in deriving the non-linear system of equations. The by-hand approach was discarded a-priori since the involved equations are cumbersome to derive and the method would be hardly scalable. The symbolic manipulation process slows down considerably when the system gets increasingly complex. In the initial modeling process, it was seen that the code was unable to handle a system with only a solar panel discretized in 3 rigid elements and with a 7 DoFs manipulator.
As an alternative, the acausal Modelica programming language was chosen. It allows to model a complex rigid bodies system using connections that do not infer any assignments but rather a relationship between variables. The model was implemented inside the Dymola environment, a third-party program using the Modelica language. The modeled system comprises the Envisat satellite, a 7 DoFs manipulator, and the chaser satellite. The overall system configuration can be visualized in figure 1, where Envisat is reported in blue, the manipulator in orange, and the chaser satellite is shown in green.

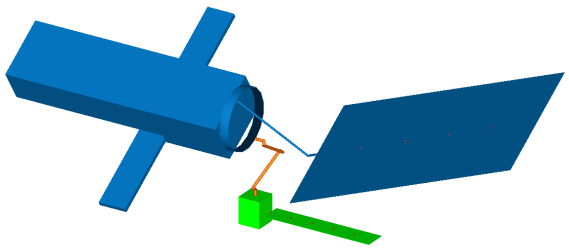

Figure 1: 3D Model visualization

3. Model validation

Since the solar panels are modeled with a lumped parameter approach, a comparison with the results of a FEM is performed to ensure the model's validity.
The validation procedure first step consists in linearizing the solar panel equations of motion. The required equations are derived using Newton-Euler formalism. The Denavit-Hartenberg parameters are then used in formulating the solar panel kinematics since they allow for the derivation of the equations using a recursive approach. The kinetic energy and the potential energy relative to each link of the solar panel are reported in equation (1).

$$\begin{aligned} T_{li} &= \frac{1}{2} m_{li} \dot{q}^T J_{pi}^T J_{pi} \dot{q} + \frac{1}{2} \dot{q}^T J_{Oi}^T R_i I_i R_i^T J_{Oi} \dot{q} \\ U_{li} &= \frac{1}{2} k_i (q_{i-1} - q_i)^2 \end{aligned} \tag{1}$$

Where q is the generalized joint variables vector. The Euler-Lagrange formalism is applied to equations (1) to obtain the non-linear dynamic equation governing the system's motion. Then, through the use of symbolic manipulation, the system of equations is reduced to a first-order system, which is then linearized in the equilibrium point described by $\dot{q} = 0_{n\times 1}$ and $q = 0_{n\times 1}$.

$$\begin{aligned} \dot{x} &= f(x) \qquad x = [\dot{q}, q]^T \\ \mathbf{A} &= \left. \frac{\partial f}{\partial x} \right|_{x=x_0} \end{aligned} \tag{2}$$

Matrix $\mathbf{A}$ represents the overall linearized system dynamics from which the eigenvalues and eigenvectors are extracted.
A FEM model is used for the comparison process. Both solar panels are discretized with 20×60 elements. The property of the elements is defined using the PCOMP, where the stacking sequence is defined by providing the thickness, orientation, and material id of each ply composing the stack. The layup is an aluminum honeycomb core sandwich with uni-directional carbon fiber layers for the upper and lower faces. The presence of the solar cell is modeled by increasing the density of the upper ply of the laminate. The solar panel model is constrained on one short edge by fixing all 6 DoFs of the nodes. The second step in the validation procedure consists of deriving the equivalent spring stiffness values. The linearized dynamics show that the torsional behavior is decoupled from the flexural one. Therefore the spring constants' derivation is carried out separately. Only one spring connected to the base of the solar panel is used to introduce the torsional dynamic. The solar

panel is modeled with five rigid elements due to limitations introduced by the symbolic manipulation process. An optimization procedure is carried out to recover the stiffnesses of the lumped spring of the simplified model. The system identification procedure reads:

$$\min_{k \in \mathcal{R}^n} e^T \mathbf{W} e \quad \text{s.t.} \quad \hat{Y} = g(k) \tag{3}$$

Where $e = (\bar{y} - \hat{y})^T$ represents the linear frequencies and shape modes error between the linearized model and the FEM. The cost criterion in eq. (3) is computed as the weighted square norm of the error vector, where the weight matrix is represented by the matrix $\mathbf{W}(w)$. The value of w is used to modify the relative weights of the frequencies with respect to the modal shapes. The approximation is performed by a Gauss-Newton method. Three different optimizations are carried out for Envisat's solar panels and the chaser. The runs differ by the weights used.
After this step, the true validation process can take place. The validation consists of the transient load analysis performed separately on Dymola and with the FEM (using Nastran). A sine weep load is applied to the tip of the solar panel. The test is run for 100 $[s]$ with 800 samples. The analysis is carried out on the tip displacement measurements, performed three times with different weight values. As the performance index, the position of the first resonance peak has been chosen, and the results are reported in table 1.

	Dymola			**FEM**
weight	1	10	0.1	–
Peak [Hz]	0.0499	0.0499	0.0798	0.0799

Table 1: Resonance frequencies

The results show that the closest match with the FEM data is the one associated with $w = 0.1$. Thus the errors due to any frequency mismatch are underweighted. The obtained spring stiffnesses are reported in table 2.

Stiffness $[Nm/rad]$				
k_1	k_2	k_3	k_4	k_5
8051	47568	15648	6884	8565

Table 2: Stiffnesses obtained from optimization with $w = 0.1$

On the other hand, the torsional spring is derived only by matching the first torsional frequency, and the resulting stiffness is $k_{tor} = 621.6$ $[Nm/rad]$.
Figure 2 shows the single-sided amplitude spectrum of the tip displacements relative to the Envisat solar panel with $w = 0.1$. As seen, the model implemented inside Dymola closely follows the behavior obtained from the FEM analysis. Femap has been used as pre and post-processing software.

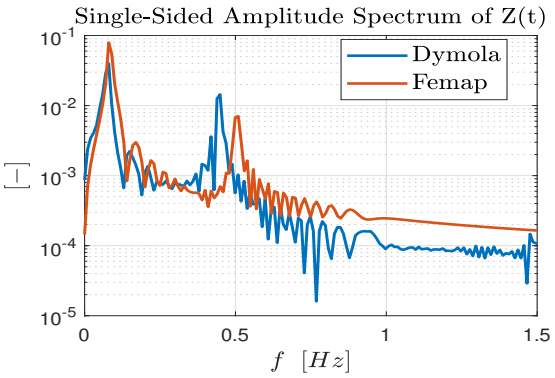

Figure 2: Transient analysis validation

The chaser solar panel validation followed the same procedure described above for the Envisat solar array. The only differences are the load magnitude, which is set to 0.01 $[N]$ instead of 1 $[N]$, and the thickness of the honeycomb core, which is decremented from 8 to 2 $[mm]$. The best match was obtained with the weights set to 0.1, and the derived spring stiffnesses are reported in table 3.

Stiffness $[Nm/rad]$					
k_1	k_2	k_3	k_4	k_5	k_{tor}
53.6	99.7	63.1	36.4	15.2	9.93

Table 3: Chaser stiffnesses with $w = 0.1$

The analysis performed on the chaser's solar panel gave worse results when compared to the previous one. This could be explained by the non-linearity of the system, which has larger effects in the smaller panel.

4. Filter implementation

Within the aim of this thesis, three different filters have been used. Regarding attitude estimation, the EKF and MEKF have been implemented. To perform the estimate of the mass

of Envisat, a modified EKF is derived. To represent the attitude of the chaser satellite, the quaternion formulation is used.
One contribution of this work is the implementation of the non-linear filtering techniques for attitude and parameter estimation in a Functional Mock-up Unit (FMU). The FMU is a file format specified by the FMI standard [1] intending to simplify the interchange of dynamic simulation models. There are two types of FMUs: model exchange and co-simulation. In this work, the second type of FMU was used since it includes both the dynamic model of the system and the numerical solver.
The filters are implemented directly inside the FMU code. The code has a predefined structure that can be divided into two distinct parts by the call to the function `fmiDoStep` [2]. This function instructs the FMU to integrate the system to the next time instant. With this knowledge, the proposed Kalman filters, characterized by a predictor and corrector step, are implemented in the FMU. The predictor step is inserted before the `DoStep` function, while the corrector step is written after. The FMU-provided functionalities are used in the filter implementation process. Before the actual implementation, the labels that refer to the quantities of interest must be identified. These labels are contained in the `ModelDescription` file along with the FMU. The above quantity labels are required for all FMU activities.
In the predictor step, the computation of the state and measurements Jacobian can be done with the function `fmiGetDirectionalDerivatives`, which provides the linearized Jacobian. Just before the call to `DoStep`, the corrected state computed at the previous time step is applied to the FMU using `fmiSetReal`.
Right after the `DoStep` code, the function `fmiGetReal` is used to extract from the FMU the predicted state and measurements. Finally, the filter's corrector step is inserted without significant modifications.
Next, the EKF and the MEKF are implemented directly without modifying their classical formulation. They differ only by the fact that the EKF uses the FMU tools for the state and measurements linearized Jacobian, while the MEKF uses predefined matrices. This difference resides in the derivation process of the MEKF. This filter is derived directly from the quaternion kinematic equation of a satellite and utilizes a state transition matrix. Thus, the MEKF utilizes the FMU-specific tools only when extracting the predicted state and measurements.
The third filter, used for the parameter estimation, is obtained by modifying the EKF. The mass is defined as strictly positive; thus, it is necessary to impose constraints on the range in which the parameter is allowed to vary. A Sigmoid function allows to apply the required constraints without major modifications to the Kalman filtering structure. The direct and inverse Sigmoid function is used, as shown in equation (4), to create a map between the state variables x to the inertial parameter θ.

$$\begin{aligned} \theta &= Sig(x) = \frac{a-b}{1-e^{-cx}} = b \\ x &= Sig^{-1}(\theta) = \frac{1}{c}\ln\left(\frac{b-\theta}{a-\theta}\right) \end{aligned} \tag{4}$$

The chaser acceleration and the manipulator joint angular acceleration are used as inputs for the mass estimation procedure. They are chosen because, as described by the `ModelDescription` file, they do depend on the inertial parameter of interest.

5. Overall model structure

The EKF and MEKF filters are used in conjunction with the parameter estimation filter. The dual estimation scheme is used where the parameter estimation filter works in parallel to the attitude filter. The dual estimate is advantageous because it is possible to write and test the filters separately before assessing the coupled stability. In addition to that, this approach allows for greater flexibility in the attitude filter implementation. For example, it is possible to use a different filter structure to the predictor-corrector one. The outputs of the attitude filters are used as the inputs of the parameter estimation filter. The estimated mass is then routed back to the attitude estimation filter. The dual estimate scheme is then inserted in the Dymola environment with the system model, as shown in figure 3.
A star tracker and a gyroscope are used and modelled as sensors.

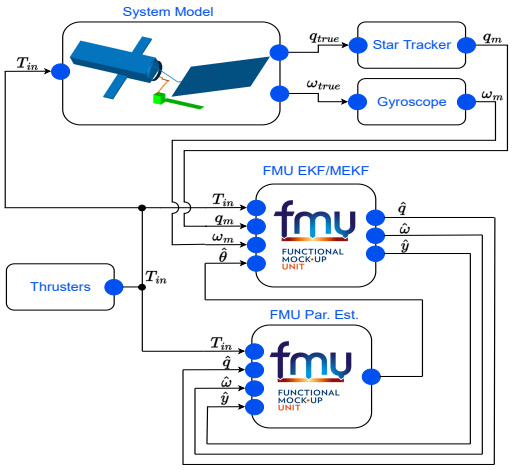

Figure 3: Overall system structure

6. Results

The attitude filter is changed between the EKF and MEKF. The system model inside the FMU is changed from a flexible model, the same one in the Dymola environment, to a model with all the springs constants set to $k = 1e+7\ [Nm/rad]$, mimicking a rigid model. Thus, for each combination, one simulation is done, for a total of four simulations.

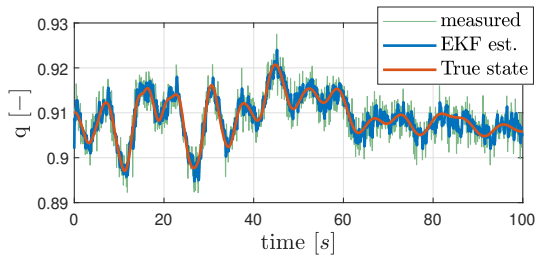

(a) Attitude estimate

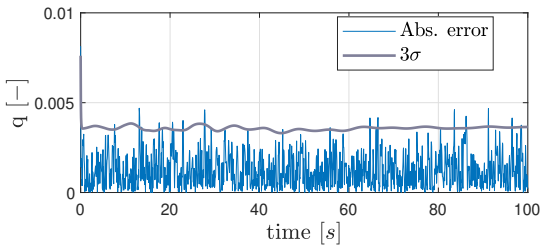

(b) Attitude estimate error

Figure 4: Fourth quaternion est. EKF

The EKF filter is tuned with $\mathbf{R}_{3\times3} = 0.01^2\mathbf{I}_{3\times3}$ $Q_{3\times3} = 0.0007^2\mathbf{I}_{3\times3}$ $P_{0,3\times3} = 0.02^2\mathbf{I}_{3\times3}$. The EKF for parameter estimation is tuned with the parameter shown in equation (5).

$$c = 0.001 \quad a = 9000\ [kg] \quad b = 5000\ [kg]$$
$$R_\theta = \begin{bmatrix} 10^{-4}\mathbf{I}_{3\times3} & \mathbf{0}_{3\times7} \\ \mathbf{0}_{7\times3} & 10^{-2}\mathbf{I}_{7\times7} \end{bmatrix} [kg^2] \tag{5}$$

The variance value assigned to the input noise added to the parameter decreases from 20.1 to 0.1 within the simulation time. The auto-covariance is large at the start of the simulation to obtain a fast convergence of the parameter estimate to the real one. Then, at the end of the simulation the variance will assume a small value to reduce the oscillation. The results relative to the EKF with the flexible model are reported in figure 4. Figure 4a shows the estimation of the fourth quaternion element. In figure 4b, the relative error with respect to the true state is compared against the confidence level derived from the covariance estimate of the filter. As seen from the results, the EKF filter with the flexible model can provide a reliable estimate for the state. In the simulation, without the parameter estimation filter, the EKF gives a less noisy estimate because there is no interaction between the two FMUs.

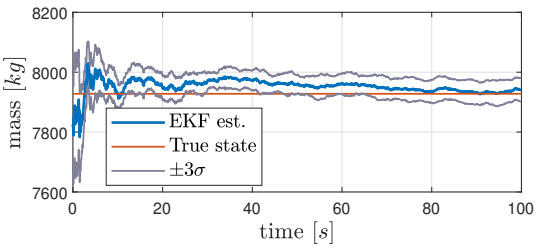

(a) Mass estimate flexible EKF

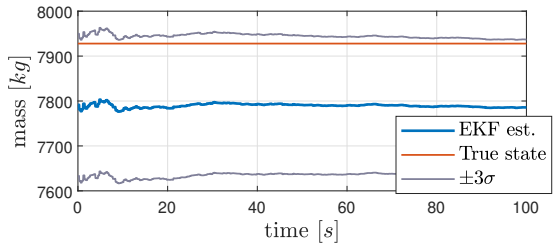

(b) Mass estimate rigid EKF

Figure 5: Mass estimate for EKF filters

The mass estimation process is carried out with an initial error of 100 $[kg]$ on the Envisat mass. Figure 5 shows the estimation results for the mass. The EKF with the flexible model converges quickly towards the true value, and, at the end of the simulation, the estimated mass

has an error of 11 $[kg]$. The EKF with the rigid body cannot estimate the inertial parameter for two main reasons: it does not use the accelerations of the manipulator's joints since it is assumed as rigid, and it utilizes an inaccurate model inside the FMU.
The MEKF results are only reported in figure 6 with the mass parameter estimation and the fourth quaternion component estimate of the flexible model. Although the filter used in the parameter estimation is the same as the previous analysis, the dual estimation scheme with the MEKF does not provide a reasonable estimate for either mass or attitude. The different implementations of the MEKF can explain this behavior. Indeed, as mentioned above, it does not utilize the FMU tools in the computation of the Jacobians. The oscillation can also be explained by the continuous variation in the Envisat estimated mass, destabilizing the MEKF. With the inaccurate data coming from the MEKF, the parameter estimation algorithm struggles to reach convergence in the simulation time.

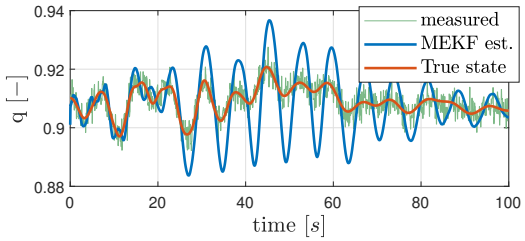

(a) Attitude estimate

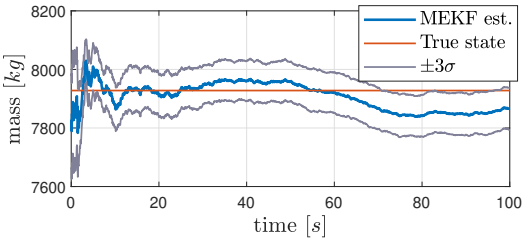

(b) Mass estimate

Figure 6: Mass and state est. MEKF

The MEKF with the rigid body implementation performed similarly to the rigid EKF analysis.

7. Conclusions

The first part of this work showed the model implementation procedure with a validation technique. The validation procedure showed that the choice of weights in the optimization procedure is fundamental to achieve a good match between the FEM and the Dymola models. It highlights that the Euler-Lagrange approach is not suited for modeling complex rigid bodies stating the usefulness of acausal programming languages. Then, a novel application of the FMI standard is demonstrated with the implementation of Kalman filtering techniques for attitude and constrained parameter estimation inside the FMU code. At last, the performance of the filters is evaluated and compared. The simulations show that the EKF outperforms the MEKF in the estimation process. This could be explained by the EKF's use of FMU specific tools. For what it concerns the rigid bodies implementation, it is clear that the simplified model, when utilized in the dual filtering scheme, does not provide a reliable estimate for the mass and, subsequently, for the attitude of the chaser satellite. In future developments, it would be advisable to implement the parameter estimation filter directly inside the attitude EKF, in order to verify whether the enlargement of the state could provide any performance improvements. This procedure cannot be done directly in the MEKF using the FMU since such filter utilizes the quaternion error as a stare and not the attitude quaternion as the EKF.

References

[1] Modelica Association Project "FMI". Functional mock-up interface specification. Online, May 2022. accessed: 21-11-2022.

[2] Scott A. Laughman, Christopher R.; Bortoff. Nonlinear state estimation with fmi: Tutorial and applications. In *American Modelica Conference*, 2020.

[3] Deshan Meng, Wenfu Xu, Chao Xu, and Zonggao Mu. Modeling and simulation study of flexible space robot for capturing large flexible spacecraft. In *Proceedings of the 32nd Chinese Control Conference*, pages 5837–5842, 2013.

[4] Deepak Raina, Sunil Gora, Dheeraj Maheshwari, and Suril V. Shah. Impact modeling and reactionless control for post-capturing and maneuvering of orbiting objects using a multi-arm space robot. *Acta Astronautica*, 182:21–36, may 2021.